ADVANCED MATERIALS INTERFACES
Open Access
www.advmatinterfaces.de

Check for updates

Tuneable Wetting of Fluorine-Free Superhydrophobic Films via Titania Modification to Enhance Durability and Photocatalytic Activity

*Julie Jalila Kalmoni, Christopher S. Blackman, and Claire J. Carmalt**

Superhydrophobic photocatalytic self-cleaning films are fabricated via aerosol-assisted chemical vapor deposition (AACVD). First, superhydrophobic/SiO_2 polymer films consisting of a combination of fatty acids, polydimethylsiloxane (PDMS) and SiO_2 nanoparticles are deposited which displayed static water contact angles >160° and maintained superhydrophobicity after 300 tape peel cycles. The AACVD process is used to achieve a highly textured morphology required for superhydrophobicity. The surface properties are then modified by depositing a thin layer of TiO_2 on the superhydrophobic coating via AACVD of titanium isopropoxide (TTIP). The deposited films are hydrophobic/superhydrophobic depending on the concentration of TTIP used in the deposition process. The resulting hybrid films exhibit enhanced photocatalytic activity relative to the uncoated superhydrophobic film, maintained hydrophobicity after exposure to toluene, and tolerated pencil hardness of up to "6H". This multi-layered approach allows to easily tune the wettability of the superhydrophobic film, which is challenging to do when the superhydrophobic and TiO_2 precursor are deposited as a single one-pot precursor.

1. Introduction

Superhydrophobic materials are water-repellent and have water contact angles (WCAs) >150°, sliding angles (SAs) <10°, and a contact angle hysteresis (CAH) that is <10°.[1,2,3] Superhydrophobicity, also known as the lotus effect, replicates the structure of lotus leaves on a synthetic scale by incorporating hierarchical roughness and a low surface energy reagent.[4,5] Superhydrophobic materials have vital real-world applications where water interaction could cause a reduction performance; examples include anti-icing, corrosion-resistance, and even in the production of biomedical materials.[6,7,8]

Such materials can be fabricated using top-down or bottom-up techniques such as templating, lithography, chemical vapor deposition (CVD), sol–gel methods, spray-coating or spin-coating.[9,10,11,12] Zhou et al. fabricated translucent superhydrophobic materials via spray-coating a one-pot mixture of PDMS, SiO_2 nanoparticles (NPs) and an acrylic resin onto murals to afford durable and UV-resistant superhydrophobic films.[13] Each deposition technique has its own benefits and drawbacks; for instance, although sol–gel methods do not require extremes of temperatures, the resulting films suffer from cracks and hence limited robustness.[14] Dip-coating occasionally produces films of uneven thickness and requires excess solvent leading to waste. Due to the nature of the spray coating process, precursors physisorb rather than chemisorb onto a substrate producing mechanically weak films. Therefore, a combination of techniques should be used to fabricate superhydrophobic materials. For instance, Huang et al. utilized a sol–gel method to produce silicic acid-coated SiO_2 NPs which were then dip-coated onto a glass substrate.[15] A dip-coat of a fluoroalkylsilane, 1H,1H,2H,2H-perfluorooctyltrichlorosilane, was carried out to afford a superhydrophobic coating with a WCA > 160°. Geng et al. fabricated a superhydrophobic film by dip-coating solid nanoparticles before spray-coating hollow silica particles and a binder to improve adherence.[16] The films were calcined at 550 °C. In both cases, a fluoroalkysilane was used, such materials pose harm to human health and the environment.[17] Therefore, there is interest in researching alternative low-surface energy reagents or deposition techniques to produce well-adhered and multifunctional superhydrophobic coatings.

The mechanism of photocatalysis consists of three stages, specifically light harvesting, creation and transportation of charge carriers, and the photocatalytic redox reactions.[18] Photocatalysis has many current and potential applications such as pollution remediation, where sunlight is used to partly or fully degrade toxins into harmless alternatives or water splitting to generate H_2 as an alternative "green" fuel. Traditional photocatalytic

J. J. Kalmoni, C. S. Blackman, C. J. Carmalt
Materials Chemistry Centre
Department of Chemistry
University College London
20 Gordon Street, London WC1H 0AJ, UK
E-mail: c.j.carmalt@ucl.ac.uk

The ORCID identification number(s) for the author(s) of this article can be found under https://doi.org/10.1002/admi.202400519

© 2024 The Author(s). Advanced Materials Interfaces published by Wiley-VCH GmbH. This is an open access article under the terms of the Creative Commons Attribution License, which permits use, distribution and reproduction in any medium, provided the original work is properly cited.

DOI: 10.1002/admi.202400519

metal oxides include ZnO, Fe_2O_3, WO_3, and more commonly, TiO_2 due to its low cost.[19] TiO_2 films are inherently hydrophilic and are fabricated by physical methods such as sputtering or chemical methods including physical vapor deposition (PVD) or CVD, with applications in photocatalysis, cancer treatment, and more recently, self-cleaning.[20] Their chemical self-cleaning ability operates by the photoexcitation of electrons from the valence band of TiO_2 (producing holes) to its conduction band.[21] This occurs if the light is of an energy that is equivalent to or larger than the band gap, which is 3.2 eV for anatase and 3.0 eV for rutile.[22]

Superhydrophobic photocatalytic self-cleaning films are a relatively new branch of self-cleaning materials, combining physical and chemical self-cleaning properties. Their physical self-cleaning abilities arises from the superhydrophobicity and the photocatalytic chemical self-cleaning property results from the photocatalytic properties of a TiO_2 film.[19] This simultaneous process is a challenge because superhydrophobicity depends on a macroscopic interaction between the surface of the film and water whereas photocatalytic activity requires a microscopic/molecular interaction (i.e., oxidation of contaminants). This synergistic combination allows the removal of liquids and degradation of organic contaminants into non-toxic molecules such as CO_2 and H_2O, enhancing the overall self-cleaning abilities of the films.[23] However, this can only be achieved if 50–70% of the surface is hydrophobic/superhydrophobic.[24] This challenge is evident in work by Ansari et al. which involved fabricating a superhydrophobic photocatalytic material by electrostatic spraying of a composite of fluorinated ethylene propylene (FEP) with SiO_2 and TiO_2 nanoparticles. Increasing the number of layers increased the hydrophobicity as this contributed to the roughness. In addition, the weight percentages of the components were explored; increasing the TiO_2 content increased the photocatalytic activity but decreased the hydrophobicity and vice versa for the SiO_2 content. Nevertheless, once optimum weight percentages were found, the material displayed tolerance to acidic/alkaline environments, good mechanical durability via a sandpaper test as well as photocatalytic abilities.[25]

Cao et al. deposited a combination of TiO_2 nanoparticles (for photocatalysis and roughness) with PFE (pentafluoroethane) functionalised with APTMS ((3-aminopropyl)trimethoxysilane) on stone substrates to provide the low surface energy, without incorporating SiO_2 NPs. Regardless, WCAs >150° were achieved as well as ultra-repellency to different solvents and emulsions and enhanced photocatalysis.[21] However, in both mentioned examples, fluorinated polymers were employed and the superhydrophobic and photocatalytic components were deposited as a single film.[25,21]

Wang et al. explored the use of solvothermal methods to prepare a ZnS superhydrophobic material which was chemically modified with stearic acid in a two-step procedure to achieve a superhydrophobic photocatalytic self-cleaning coating. Even with the surface-modified ZnS coating, the material displayed enhanced photocatalytic degradation relative to the unmodified ZnS coating due to its ability to reduce electron-hole pair recombination.[19]

Superhydrophobic TiO_2 films can display both types of self-cleaning properties – physical and chemical respectively, in tandem. Therefore, the aim of this study is to combine both layers to produce a superhydrophobic photocatalytic self-cleaning coating and determine how its resultant properties change as the thickness of the TiO_2 film increases relative to a TiO_2 film deposited in the same conditions but on a fluorine-doped tin oxide (FTO) float glass substrate. This was carried out using aerosol-assisted chemical vapor deposition (AACVD) to both deposit a superhydrophobic polymer film and to modify the resultant surface with TiO_2 due to its chemical durability and excellent photocatalytic activity. The steps within the AACVD process include the generation of aerosols via an ultrasonic humidifier, the transportation of these droplets to the heated rig, and the homogenous or heterogeneous reaction of the precursor in the gas phase or with the substrate, respectively. Relative to traditional CVD, the AACVD method can deposit relatively inexpensive polymeric solutions with a relatively small and cheap setup. AACVD is a potentially scalable technique and depends on the solubility of precursors and not their volatility.[26] Relative to spray coating and dip coating, there are more parameters that can be varied to produce optimum films such as the deposition duration, temperature, carrier gas flow rates as well as precursor composition.[27]

Polydimethylsiloxane (PDMS) was used in the fabrication of the superhydrophobic film because it does not hinder the photocatalytic properties of the TiO_2 film and it is a low surface energy reagent.[2] Unlike most research, TiO_2 was deposited as a separate film rather than being incorporated within the superhydrophobic precursor mix; the precursor used was titanium isopropoxide dissolved in anhydrous toluene. There are many advantages of this novel multi-layer process of Superhydrophobic (SH), and TiO_2 films over incorporating TiO_2 into the SH precursor mixture as the latter makes it difficult to alter the hydrophobicity or surface chemistry of the film.[28] Work by Diesen et al. confirms that TiO_2 films deposited on glass substrates are hydrophilic with water contact angles of 82°.[29] However, while a PDMS and SiO_2 film produces a superhydrophobic film, the surface can be tuned by dual layers (and the order of the layers). For example, work by Liu et al. transformed hydrophobic TiO_2 into superhydrophobic-TiO_2 by adding PDMS as a thin second film of ≈2.2 nm on the TiO_2 undercoating.[30] Also, the incorporation of TiO_2 into a SH precursor mixture may not enhance the durability of the film as much as a separate layer of TiO_2 which could provide a layer of protection for the coating. In addition, a coating of TiO_2 on the surface may have enhanced photocatalytic properties relative to a film with a one-pot hybrid mixture of TiO_2/PDMS/SiO_2. Furthermore, many coatings are produced by a sol–gel method however, the novelty within the research of this paper is that we use a different, potentially scalable technique.[31]

2. Results and Discussion

To determine the effect of depositing a TiO_2 film (inherently superhydrophilic) on top of a superhydrophobic film, various volumes of titanium(IV) isopropoxide (TTIP) were deposited on superhydrophobic films formed via AACVD at 350 °C (**Figure 1**). The superhydrophobic film consisted of SiO_2 NPs to provide roughness, cured polydimethylsiloxane (PDMS) and equal masses of stearic acid (SA) and palmitic acid (PA) to provide the low surface energy, as reported previously.[12] Both roughness and low surface energy are required for superhydrophobicity.[32] The superhydrophobic film was deposited by AACVD via

© 2024 The Author(s). Advanced Materials Interfaces published by Wiley-VCH GmbH

21967350, 2024, 35, Downloaded from https://advanced.onlinelibrary.wiley.com/doi/10.1002/admi.202400519 by Test, Wiley Online Library on [23/07/2025]. See the Terms and Conditions (https://onlinelibrary.wiley.com/terms-and-conditions) on Wiley Online Library for rules of use; OA articles are governed by the applicable Creative Commons License

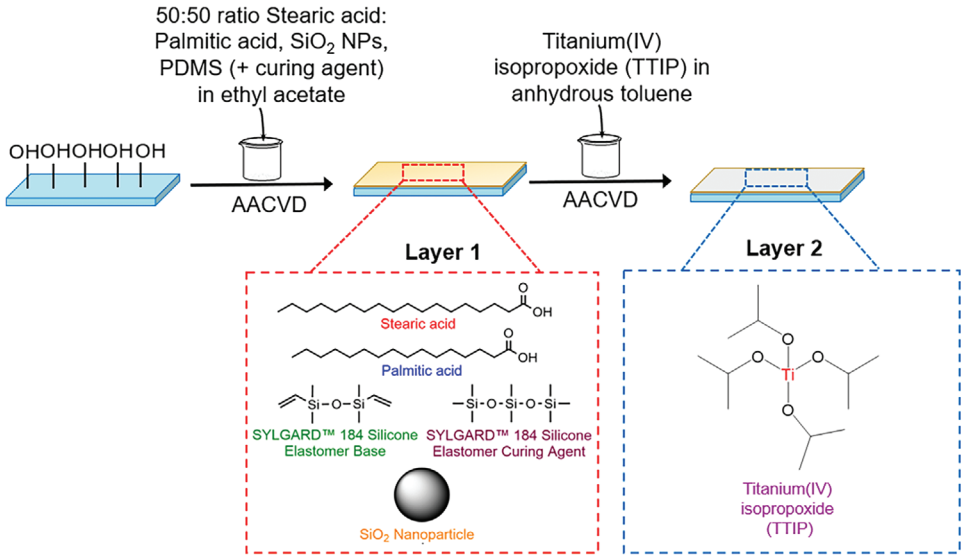

Figure 1. Schematic of the fabrication of the fluorine-free superhydrophobic (SH) material and its resultant surface modification via TiO_2 deposited via AACVD.

thermophoretic effects where the gas-phase precursor impacts the cooler glass substrate above the carbon block rather than the substrate on the heated carbon block.[33]

To achieve full coverage of the superhydrophobic coatings by the TiO_2 thin film, the superhydrophobic films underwent plasma surface treatment before depositing the TTIP precursor to create more -OH groups for the metal oxide precursor to react with and to start nucleation. Differences in TiO_2 coverage were inferred by the size of the standard deviation (taken to be the variance of coverage) of the water contact angles. After plasma treatment, the superhydrophobic films became superhydrophilic, making it difficult to measure the water contact angle. Altering the volumes of TTIP led to varying levels of hydrophobicity from superhydrophobic to hydrophilic, as shown in **Table 1**. SH/TiO_2/0.4, consisted of 0.4 mL of TTIP deposited onto the superhydrophobic film via AACVD and SH/TiO_2/1.4 consisted of 1.4 mL of TTIP deposited onto the superhydrophobic film; the films had WCAs of 142 ± 26° and 70 ± 3°, respectively. This is a contrast to their counterparts, film TiO_2/0.4 (65 ± 0°) and TiO_2/1.4 (77 ± 4°), both consisting of TTIP deposited on FTO float glass substrates via AACVD at 350 °C. The film thicknesses of these counterparts were measured via ellipsometry. Film TiO_2/0.4 has a thickness of 80 nm and film TiO_2/1.4 has a film thickness of 510 nm. The thickness of the SH/TiO_2 films could not be accurately measured using the same instrument due to the complexity of the underlying superhydrophobic film. However, we assumed TiO_2 thicknesses ranging from 80–510 nm on the superhydrophobic counterparts (i.e., SH/TiO_2 films).

Table 1. The conditions used to deposit the TiO_2 film on the superhydrophobic films via AACVD along with the resulting water contact angles and transmittance.

Film name	Volume of TTIP [cm^3]	WCA [°]	T at 400–800 nm [%]
Superhydrophobic (SH)	0	165 ± 2	34
TiO_2/0.4	0.4	65 ± 0	74
TiO_2/1.4	1.4	77 ± 4	65
SH/TiO_2/0.4	0.4	142 ± 26	28
SH/TiO_2/0.5	0.5	143 ± 14	24
SH/TiO_2/0.6	0.6	94 ± 11	21
SH/TiO_2/0.8	0.8	83 ± 8	7
SH/TiO_2/1	1	73 ± 6	19
SH/TiO_2/1.2	1.2	82 ± 2	16
SH/TiO_2/1.4	1.4	70 ± 3	9

Less variability in the WCA was observed when TTIP was deposited on FTO float glass substrates relative to when TTIP was deposited on a superhydrophobic film (Table 1). The SH/TiO_2 films were studied and characterized via X-ray photoelectron spectroscopy (XPS), Raman spectroscopy, FT-IR, X-ray diffraction (XRD), scanning electron microscopy/electron dispersion microscopy (SEM/EDS), and UV–vis. Their functional properties, photocatalytic properties, mechanical durability, and self-cleaning abilities were also measured.

XPS, a surface-sensitive technique, indicated the presence of C, O, Si, and Ti as expected, with a SH/TiO_2 survey spectrum provided in the supplementary information, S1. The C, O, Si, and Ti spectra for all SH/TiO_2 films were similar with an example shown in **Figure 2** for film SH/TiO_2/1.4. Little Si was evident, indicating very little breakthrough of the underlying superhydrophobic film. Similarly, carbon on the surface of the film was minimal, except for the prominent peak at 285.0 eV. The deconvoluted O 1s spectrum highlights the presence two peaks, O bound to Ti (530.5 eV) and O attached to the surface of TiO_2 (532.2 eV), i.e., adsorbed water.[34,35] Any deviations of fit are caused by minor contributions from C and Si. For the O1s fit, contributions from C1s and Si have been ignored as their contributions are so low. The Ti 2p XPS scan, has a sharp $2p_{3/2}$ peak at 459.2 eV, indicating that TiO_2 has been successfully deposited.[36,37]

© 2024 The Author(s). Advanced Materials Interfaces published by Wiley-VCH GmbH

21967350, 2024, 35, Downloaded from https://advanced.onlinelibrary.wiley.com/doi/10.1002/admi.202400519 by Test, Wiley Online Library on [23/07/2025]. See the Terms and Conditions (https://onlinelibrary.wiley.com/terms-and-conditions) on Wiley Online Library for rules of use; OA articles are governed by the applicable Creative Commons License

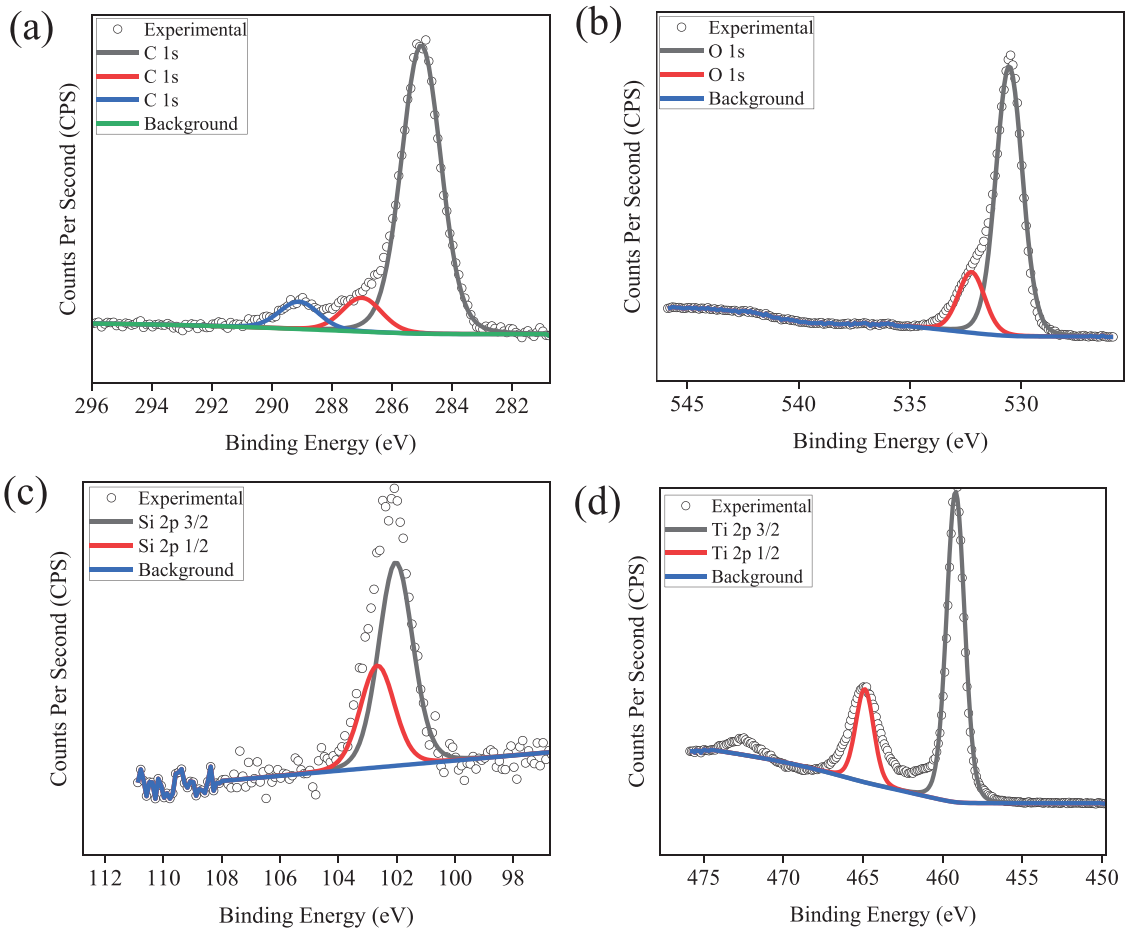

Figure 2. X-ray photoelectron (XPS) surface scans for film SH/TiO_2/1.4 showing the a) C 1s, b) O 1s, c) Si 2p, and d) Ti 2p spectra at 0 nm.

FTIR of a film before and after depositing TiO_2 via AACVD (Figure S2, Supporting Information) indicated peaks representative of the Ti–O–Ti bridge stretching vibrations and the Ti–O stretching mode within the 800–400 cm^{-1} region.[38] The characteristic peaks indicative of the underlying superhydrophobic film were observed for the films with lower [TTIP].[12]

Raman spectroscopy (**Figure 3**) was used to confirm that the TiO_2 films were anatase with peaks at 144 cm^{-1} (E_g), 198 cm^{-1} (E_g), 397 cm^{-1} (B_{1g}), 515 cm^{-1} (A_{1g}), and 637 cm^{-1} (E_g).[18] In addition to Raman spectroscopy, all the peaks in the PXRD pattern (**Figure 4**) confirm the presence of TiO_2 (anatase phase), no TiO_2 rutile phase was evident. These peaks are: 25.3°, 37.1°, 37.9°, 38.6°, 48.1°, 53.9°, 55.2°, 62.8°.[39]

The SEM images of the uncoated superhydrophobic films indicate networks of uneven and irregularly shaped microparticles with sizes varying from 1 to 9 µm (**Figure 5**). However, it was evident that as the concentration of TTIP increased, clusters coating the polymer particles emerge, filling the matrix and reducing the roughness. For film SH/TiO_2/1.2, most of the particle ranged from 2–3 µm although larger aggregates of these smaller particles reached ≈6 µm in size. It is evident from the SEM images that film SH/TiO_2/1.2 has a much flatter topology than the SH film without the TiO_2 overcoat.

TiO_2 has a high surface energy (1.28 J m^{-2}) relative to PDMS (a component of the superhydrophobic film), with a surface

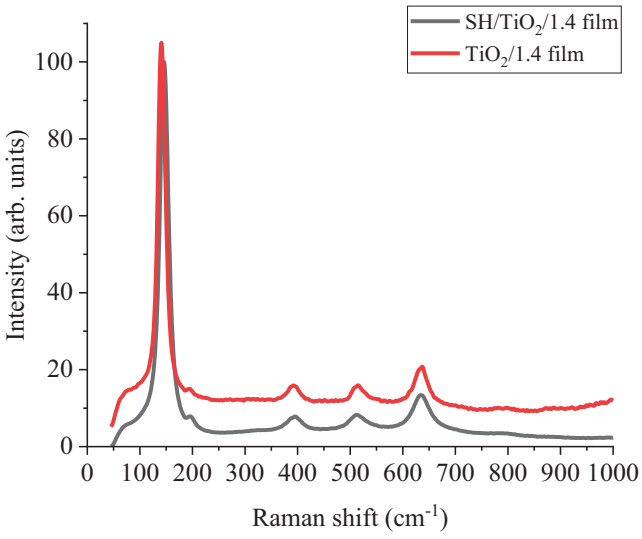

Figure 3. Raman spectrum of the SH/TiO_2/1.4 film and TiO_2/1.4 film.

© 2024 The Author(s). Advanced Materials Interfaces published by Wiley-VCH GmbH

21967350, 2024, 35, Downloaded from https://advanced.onlinelibrary.wiley.com/doi/10.1002/admi.202400519 by Test, Wiley Online Library on [23/07/2025]. See the Terms and Conditions (https://onlinelibrary.wiley.com/terms-and-conditions) on Wiley Online Library for rules of use; OA articles are governed by the applicable Creative Commons License

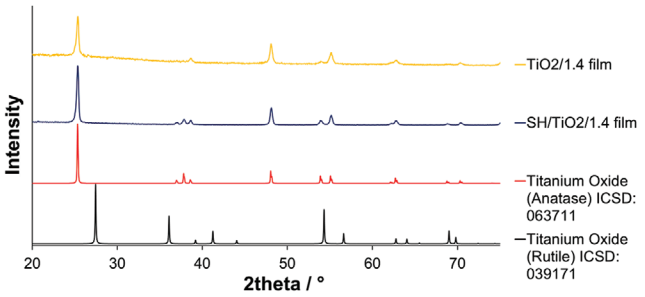

Figure 4. PXRD pattern of films TiO_2/1.4 and SH/TiO_2/1.4, indicative of the TiO_2 anatase phase and absence of the rutile phase.

energy of 19–21 mJ m^{-2}, which could contribute to the reduction in superhydrophobicity, even at low concentrations of TTIP.[40,41]

As well as the rough morphology, the varying thicknesses of the films were also attributed to the roughness of the SH film, a requirement for such coatings. Variations in superhydrophobicity and root-mean-square roughness (Sq) resulted in variable thicknesses as seen in the variable transmittance percentages (Tables 1 & 2). Generally, as the thickness increases, the percentage transmittance decreases however, the inconsistent % transmittance values are due to the rate of the AACVD process, which was relatively high, making precise control of the thickness of the film more challenging.

Comparing the static WCAs of the films, generally, as the thickness of the TiO_2 film increases, the WCAs decrease (Table 1). Similarly, on reaching a certain thickness of TiO_2 deposited on the superhydrophobic film (e.g., film SH/TiO_2/1.4), the WCA becomes that of pure TiO_2 deposited on glass, as the underlying superhydrophobic film does not influence the WCA. There were slight variations in the WCA across the uncoated SH film (from 157° to 160°), indicating superhydrophobicity. Greater variations in WCA were observed when TTIP was deposited on top of all the SH films which may be due to difficulties in covering the rough surface.

The contact angle hysteresis (CAH) was measured to determine the homogeneity and smoothness of the film. Smoother surfaces display lower CAH due to reduced lateral energy barriers and hence lower friction, with superhydrophobic materials exhibiting a greater CAH due to their increased roughness.[42] In this case, the CAH of the films decreases as the thickness of the TiO_2 film increases, with a large drop in CAH going from 1.2 mL of TTIP (film SH/TiO_2/1.2) to 1.4 mL of TTIP (film SH/TiO_2/1.4). This could potentially be due to some areas remaining superhydrophobic which is evident in the large differences/variance in standard deviation of the WCAs or due to the large differences in the sizes of the TiO_2 clusters and hence roughness of the films. Linking this to the root-mean-square (roughness) values, there is an observable link between roughness and the contact angle hysteresis during sequential reduction in TiO_2 film thickness/TTIP concentration. However, at the middle-range concentrations of TTIP used, namely from films SH/TiO_2/0.5 up to and including, SH/TiO_2/1, we do not observe significant changes to the roughness with increasing TiO_2 thickness as the film is conformal. At higher concentrations the TiO_2 begins to smooth the surface, filling the gaps in the matrix and hence reducing the roughness.

Stearic acid degradation tests were pursued to investigate the photocatalytic activity where the films were soaked in a stearic acid solution, exposed to UV light, and FT-IR scans were taken at regular intervals (**Figure 6**). The mechanism for stearic acid degradation involves the photogeneration of electrons and holes in the TiO_2 (anatase) film on absorbing UV light with an energy ≥ ca. 3.2 eV.[22] The electrons and holes travel through to the stearic acid coating where, with oxygen, initiate photocatalytic redox reactions, producing CO_2 and H_2O.[43] Occasionally, some of the charge carriers may recombine, which is unfavorable.

For the superhydrophobic film with no TiO_2 (film SH), there was a 42% reduction in stearic acid coverage during the test period. For SH/TiO_2/0.4, a 52% reduction in stearic acid coverage was observed and for SH/TiO_2/1.4, this was 65%; these two films were studied due to using the lowest and highest concentrations of TTIP for the deposition of the TiO_2 layer, respectively. There was a greater initial reduction in stearic acid coverage for the SH/TiO_2/0.4 film from time 0 h to time 0.5 h relative to the SH/TiO_2/1.4 film however, after this time (0.5 h until 30 h), the continued reduction in both films was similar. The TiO_2/0.4 and the SH films display similar overall reductions in stearic acid coverage indicating the photocatalytic oxidation of stearic acid by oxygen and that the TiO_2 film for TiO_2/0.4 is very thin.

Hence, the greater the thickness of the TiO_2 layer, the greater the reduction in stearic acid coverage although the rate of reduction did not vary significantly across the three films. These results confirm the enhanced degradation of stearic acid hence photocatalytic chemical self-cleaning abilities whilst displaying hydrophobicity. It is surprising that the photocatalytic activity of TiO_2/1.4 is lower than that of TiO_2/0.4 however, the photocatalytic activity has been shown previously to be dependent on the thickness of the TiO_2 film as increased thickness leads to the increased recombination rate of photocarriers. TiO_2 thin films of 2.6–260 nm, deposited via atomic layer deposition (ALD), displayed the highest photocatalytic activity with a thickness of 130 nm.[44] In our case, films TiO_2/0.4 and TiO_2/1.4 had film thicknesses of 80 and 510 nm, respectively. Films TiO_2/0.4 and TiO_2/1.4 had less of a reduction in stearic acid coverage relative to the SH/TiO_2 films specifically due to the smooth morphology of the pure TiO_2 films (Figure S3, Supporting Information), also confirmed by the low S_q values (**Table 2**), leading to a reduced surface area. The increased roughness and topology on the surface of the SH/TiO_2 films will likely lead to an increase in surface area. The SEM image of SH/TiO_2/1.4 (Figure 5, image d) demonstrates that the initial topology of the SH film is retained, along with rafts of TiO_2 deposition, the TiO_2 film does not completely flatten the film, also confirmed by the S_q value of 0.18 ± 0.03. In contrast, the SEM image of film TiO_2/1.4 (Figure S3, Supporting Information), indicates similar particulate morphology but without the large features; overall this film is smooth. It has been previously reported that the presence of nano-cracks in the thin films can improve their photocatalytic performance; these cracks are evident in the SEM images of film SH/TiO_2/1.4 (Figure S6, Supporting Information) but not TiO_2/1.4 (Figures S3 and S5, Supporting Information) Figure 6.[45]

Robustness testing was carried out to determine the effect of the TiO_2 layer on the durability of the films. Here, we focused on testing the films with two contrasting concentrations of TTIP, namely SH/TiO_2/0.4 and SH/TiO_2/1.4.

© 2024 The Author(s). Advanced Materials Interfaces published by Wiley-VCH GmbH

21967350, 2024, 35, Downloaded from https://advanced.onlinelibrary.wiley.com/doi/10.1002/admi.202400519 by Test, Wiley Online Library on [23/07/2025]. See the Terms and Conditions (https://onlinelibrary.wiley.com/terms-and-conditions) on Wiley Online Library for rules of use; OA articles are governed by the applicable Creative Commons License

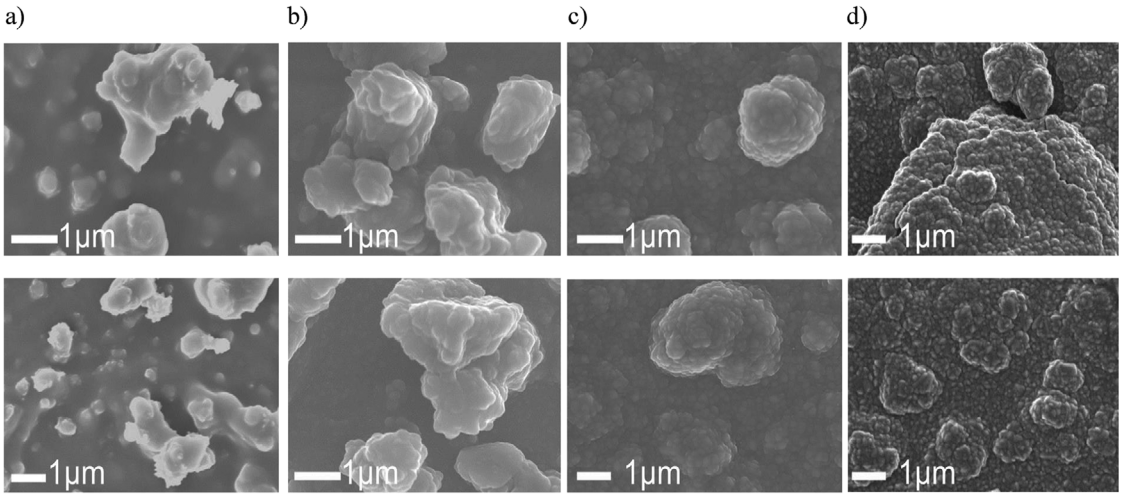

Figure 5. SEM images of the morphologies of the films with increasing concentrations of TTIP in the precursor mixture. Image a) Superhydrophobic film without a TiO_2 coating b) SH/TiO_2/0.4 c) SH/TiO_2/0.8 d) SH/TiO_2/1.2.

The films were exposed to toluene (highly apolar) and ethanol (highly polar) for a period of 5 h with WCAs measured every hour, **Figure** 7a,b. On exposure to both solvents, SH/TiO_2/0.4 was initially superhydrophobic but became borderline hydrophobic (within the limit of error). There was only a ≈4° decrease in WCA from 0 to 5 h on exposure to toluene and a ≈7° reduction on submerging the film to ethanol. For SH/TiO_2/1.4, this was an 11° reduction in toluene and a 28° reduction in ethanol for the same period. In both cases, a greater decrease in WCA was observed in ethanol rather than toluene as the ethanol dissociatively adsorbs on the TiO_2. The ethoxides attach to the surface metal cations but the hydrogen ions attach to the surface oxygen anions forming surface hydroxyls.[46] The presence of hydroxyl groups reduces the WCA. We observe a comparatively larger reduction in WCA for film SH/TiO_2/1.4 relative to SH/TiO_2/0.4 due to the thicker TiO_2 film. The uncoated SH film had the smallest decrease in WCA on exposure to both solvents.

Both films showed a reduction in WCA on exposure to UV light for 15 days, Figure 7c. Carboxylic acids and other hydrophobic particles present in the surrounding environment bind to the TiO_2 layer due to its bidentate bonding abilities and oxygen vacancies, making the films hydrophobic. However, on exposure to UV light, these organic molecules are photocatalytically decomposed, inducing hydrophilicity (for film SH/TiO_2/1.4), relative to the uncoated SH film without the TiO_2 overlayer, where the WCA does not change.[20]

Three untested pieces of films SH, SH/TiO_2/0.4, and SH/TiO_2/1.4 were annealed in a furnace at 300 °C for 5 h to determine their heat durability. Overall, there was only a 6° decrease in WCA for the uncoated SH film, a 10° decrease in WCA for SH/TiO_2/0.4 but a significant reduction in WCA of ≈27° for

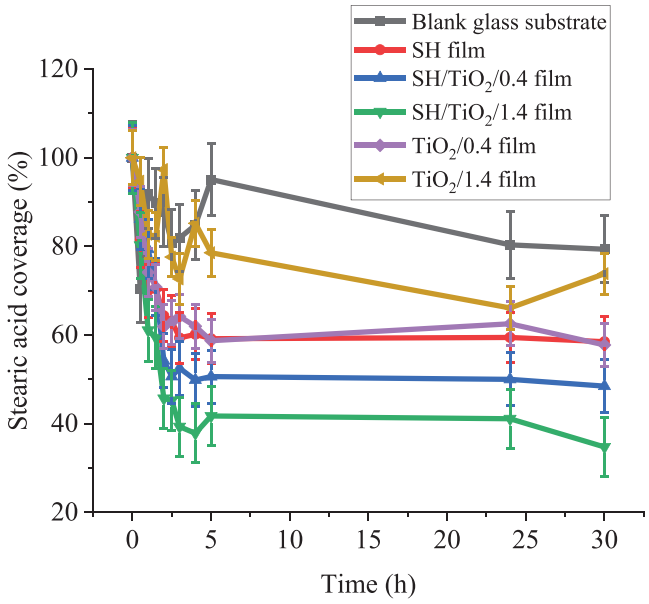

Figure 6. Graphical representation of the photocatalytic activities (by measuring the stearic acid coverage reduction) of film SH (without a TiO_2 film), the SH/TiO_2 films, and the TiO_2 films (without the underlying superhydrophobic film).

Table 2. The contact angle hysteresis (CAH) and Root-mean-square-height, Sq of a superhydrophobic film prior to TiO_2 deposition, the TiO_2 controls, and SH/TiO_2 films.

Film	Volume of TTIP [cm^3]	CAH [°]	RMS height, Sq [μm]
Superhydrophobic (SH)	0	20 ± 6	0.28 ± 0.03
TiO_2/0.4	0.4	22 ± 14	Immeasurable
TiO_2/1.4	1.4	24 ± 12	0.20 ± 0.04
SH/TiO_2/0.4	0.4	23 ± 8	0.27 ± 0.03
SH/TiO_2/0.5	0.5	22 ± 7	0.24 ± 0.07
SH/TiO_2/0.6	0.6	23 ± 8	0.24 ± 0.02
SH/TiO_2/0.8	0.8	21 ± 7	0.24 ± 0.04
SH/TiO_2/1	1	21 ± 7	0.26 ± 0.01
SH/TiO_2/1.2	1.2	22 ± 8	0.20 ± 0.07
SH/TiO_2/1.4	1.4	14 ± 6	0.18 ± 0.03

© 2024 The Author(s). Advanced Materials Interfaces published by Wiley-VCH GmbH

21967350, 2024, 35, Downloaded from https://advanced.onlinelibrary.wiley.com/doi/10.1002/admi.202400519 by Test, Wiley Online Library on [23/07/2025]. See the Terms and Conditions (https://onlinelibrary.wiley.com/terms-and-conditions) on Wiley Online Library for rules of use; OA articles are governed by the applicable Creative Commons License

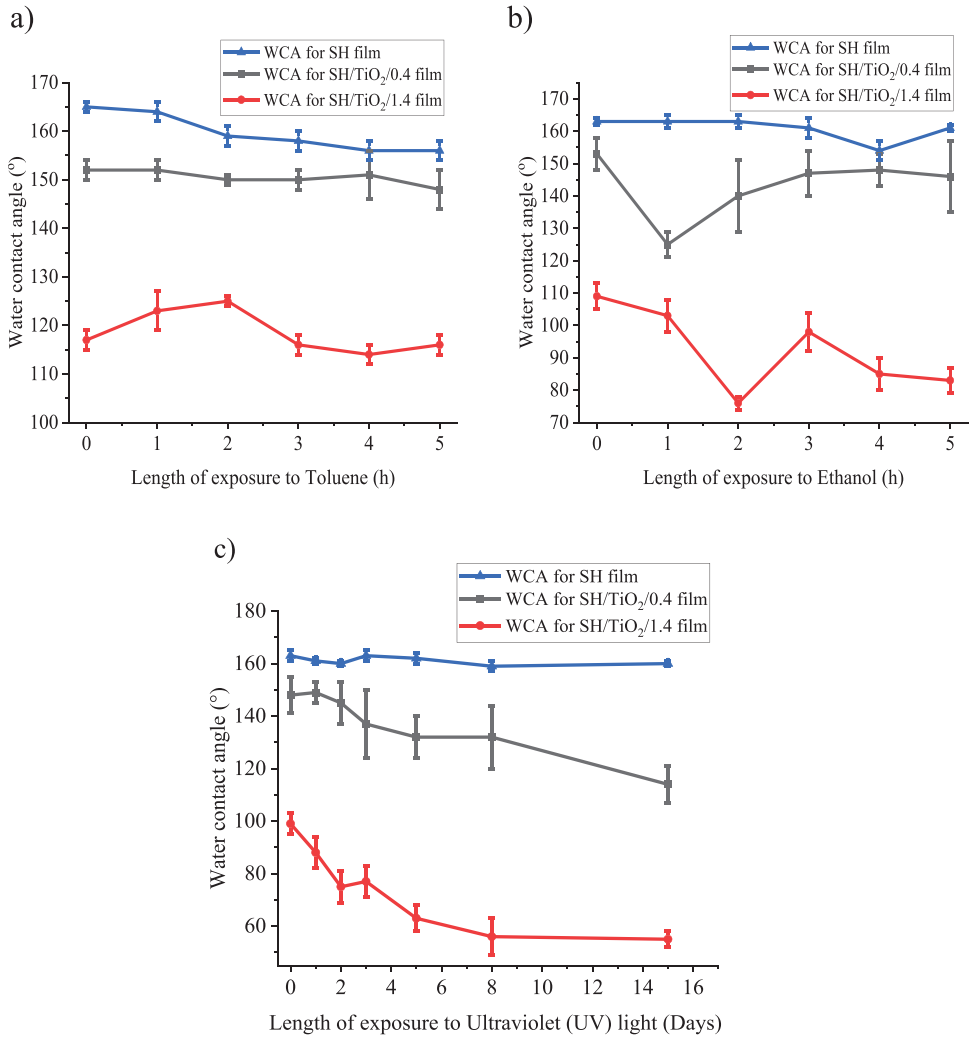

Figure 7. Changes in the water contact angles of the uncoated SH film, SH/TiO_2/0.4 and SH/TiO_2/1.4 on 5 h of exposure to a) Toluene and b) Ethanol and c) on 15 days of exposure to Ultraviolet (UV) light.

SH/TiO_2/1.4. A reason for the reduction in water contact angle could be due to the removal of carbon contaminants on the surface which can contribute to hydrophobicity due to its roughness and low surface energy.[20] The carbon contamination may have arisen from the decomposition of the precursors or from other pollutants in the air which can be removed with annealing. Studies by Gorthy et al. indicated that heat treatment <600 °C in the air did not impact the phase or morphology of the TiO_2 films but instead removed the carbon content.[47]

A tape peel test was carried out where tape was repeatedly stuck onto the film and removed to determine its mechanical durability. Film SH/TiO_2/0.4 had a smaller reduction in WCA of ≈15° compared to SH/TiO_2/1.4 which had a reduction of ≈20°. The decrease and then increase in WCA could be due to the removal of the TiO_2 film and hence exposure of the underlying superhydrophobic layer. The repeated tape peel cycles made the films stickier, causing the water droplets to penetrate in the grooves of the film, formed during the tape peel test, which can be visualized in **Figure 8**. Figure 8 is an EDS scan of the middle of film SH/TiO_2/1.4, after the tape peel test. There are light and dark-colored particles, with more spots visible on the darker particles in the Si Kα and O Kα scans; these are assumed to be the superhydrophobic underlayer as they are not covered in dots in the Ti Kα scan. SEM images of the middle film SH/TiO_2/1.4, prior to the tape peel test can be found in the supplementary information (Figure S4, Supporting Information).

The EDS scans of SH/TiO_2/1.4 after the tape peel test (at the edge of the film), **Figure 9**, displays a greater reduction in Ti indicating that it is easier to remove the TiO_2 layer here than from the middle of the film. Clear differences in the elemental composition following tape removal are visible in Figure 9 due to visible differences in Si and Ti spot numbers across the film. The coverage of carbon remains even across the film, the oxygen coverage concentrates on the exposed superhydrophobic region and so does the silicon. The titanium remains concentrated on the TiO_2 area that has not been removed by the tape. Shadowing is particularly evident in the O Kα scans (Figures 8b and 9b), even with increased electron beam voltage and scan length. This is due to the Ti overlayer suppressing the omission of x-rays from the underlying superhydrophobic layer. Similarly, the geometry of the

© 2024 The Author(s). Advanced Materials Interfaces published by Wiley-VCH GmbH

21967350, 2024, 35, Downloaded from https://advanced.onlinelibrary.wiley.com/doi/10.1002/admi.202400519 by Test, Wiley Online Library on [23/07/2025]. See the Terms and Conditions (https://onlinelibrary.wiley.com/terms-and-conditions) on Wiley Online Library for rules of use; OA articles are governed by the applicable Creative Commons License

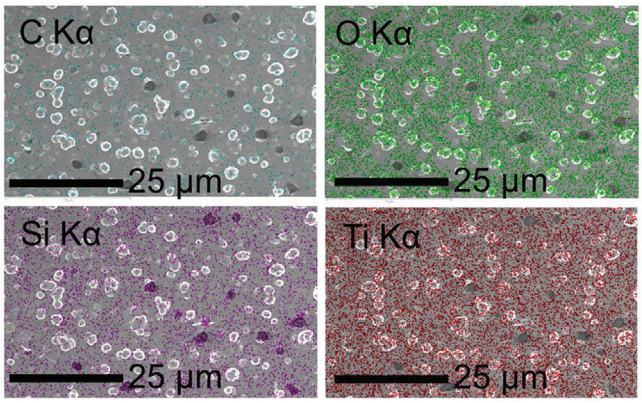

Figure 8. EDS layered images of film SH/TiO_2/1.4 after the tape peel test, specifically the middle of the film; Carbon Kα, Oxygen Kα, Silicon Kα, and Titanium Kα.

EDS instrument (i.e., the detector being offset from the film) is also a contributing factor.

A clear scratch was visible in the coating of film SH/TiO_2/0.4, after using Pencil Hardness H (Figure S7, Supporting Information). However, film SH/TiO_2/1.4 tolerated the hardest pencil, 6H which created a debris-filled scratch indicating the film's ability to tolerate pencils with even greater hardness. This is due to SH/TiO_2/1.4 having a thicker TiO_2 coating than SH/TiO_2/0.4. The uncoated SH film tolerated a pencil hardness of F indicating improved robustness due to TiO_2 film.[12] The robustness of the films can be explained by the deposition process; AACVD of TiO_2 is akin to conventional CVD as it involves a heterogeneous reaction of the vapor with a substrate, forming a chemical bond across the interface (i.e., chemisorption) rather than thermophoresis which involves physisorption of particles.[33,48] Fu et al. spray-coated a superhydrophobic precursor comprised of fluorinated polyurethane-coated SiO_2 NPs, carbon nanotubes, and PDMS with a tolerable hardness of "4H."[49] Although the film exhibited impressive robustness, it employed the use of a harmful fluorinated reagent. On the other hand, our work shows that we can enhance the robustness of a fluorine-free film with the use of a metal oxide.

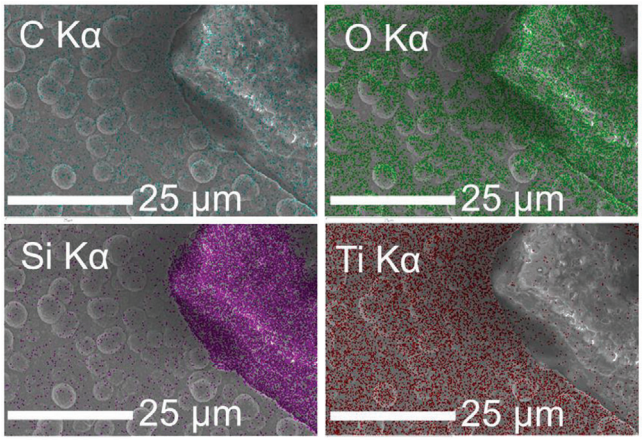

Figure 9. Layered EDS images of film SH/TiO_2/1.4 after the tape peel test, specifically the edge of the film; Carbon Kα, Oxygen Kα, Silicon Kα, and d) Titanium Kα.

Methylene blue was pipetted onto the films to determine their self-cleaning abilities (Figure S8, Supporting Information). SH/TiO_2/0.4 retained some self-cleaning abilities with the methylene blue droplet readily rolling off the surface and with a sliding angle of ≈6°. The film with the highest concentration of TTIP deposited, SH/TiO_2/1.4, displayed limited self-cleaning abilities and a sliding angle of ≈18°, with the droplets readily sticking to the surface. However, in both cases, reduced physical self-cleaning abilities were compensated by enhanced chemical self-cleaning abilities relative to the uncoated SH film which displayed excellent physical self-cleaning properties but limited chemical self-cleaning properties, determined by pipetting methylene blue on the surface and the stearic acid degradation test, respectively.

3. Conclusion

In this study, a superhydrophobic film consisting of PDMS, stearic acid, palmitic acid, and SiO_2 nanoparticles were surface-modified with TiO_2 (anatase) via the AACVD of TTIP at 350 °C. SEM indicated the formation of clusters which increased as the concentration of TTIP increased. Photocatalytic testing and WCA measurements revealed the film's ability to display dual functionality of chemical and physical self-cleaning abilities and enhanced photocatalytic activity relative to TiO_2 films without the SH undercoating. On exposure to ethanol and UV light, the films displayed reductions in WCAs due to the formation of hydroxyl groups. The films maintained hydrophobicity on exposure to toluene, tape peels and displayed tolerance to "harder" pencils relative to the uncoated SH film due to the addition of a thin layer of TiO_2, improving the SH film's overall durability. Even a very thin film of TiO_2 can improve the robustness as seen with film SH/TiO_2/0.4. Previous studies have shown that incorporating TiO_2 nanoparticles into the superhydrophobic precursor mixture are needed to create superhydrophobic photocatalytic self-cleaning films. However, our work is evidence that TiO_2 can be deposited as a separate film onto a superhydrophobic film to achieve the same property. This work confirms that we can produce hydrophobic-TiO_2 films via a layer-by-layer deposition by tuning the surface chemistry of a superhydrophobic film via AACVD.

4. Experimental Section

Materials: Vinyl-terminated polydimethylsiloxane (PDMS), namely Sylgard-184 Silicone Elastomer Base, and its respective curing agent were purchased from Dow Corning. Aerosil OX50 fumed SiO_2 nanoparticles (NPs) were purchased from Lawrence Industries. Stearic acid (SA, reagent grade, 95%), palmitic acid (PA, ≥99%), and ethyl acetate (laboratory grade) were purchased from Sigma Aldrich. Titanium(IV) isopropoxide (97%) and anhydrous toluene (99.8%) were purchased from Sigma Aldrich without further purification. Table 1 describes the details of the various volumes of titanium(IV) isopropoxide used. SiO_2 barrier-coated fluorine-doped tin oxide (FTO) glass substrates (FTO) float glass was provided by Pilkington NSG and cut to 150 mm × 40 mm × 3 mm for AACVD. N_2 (99.99%) was supplied by BOC.

A Henniker plasma cleaner (HPT-100) was used to plasma treat the surface of the superhydrophobic film with the following parameters: a gas flow of 2 sccm and a duration of 4 min.

© 2024 The Author(s). Advanced Materials Interfaces published by Wiley-VCH GmbH

21967350, 2024, 35, Downloaded from https://advanced.onlinelibrary.wiley.com/doi/10.1002/admi.202400519 by Test, Wiley Online Library on [23/07/2025]. See the Terms and Conditions (https://onlinelibrary.wiley.com/terms-and-conditions) on Wiley Online Library for rules of use; OA articles are governed by the applicable Creative Commons License

Film Synthesis—Fabrication of the Superhydrophobic Film: Stearic acid (0.20 g), palmitic acid (0.20 g), Sylgard-184 (0.15 g), OX50 SiO_2 NPs (0.25 g) and its respective curing agent (0.02 g) were dissolved in ethyl acetate (60 cm^3) for 20 min. This precursor mixture was deposited onto a glass substrate via AACVD. The set-up had a bottom-down heating configuration, with the film deposited on the glass top plate (substrate). The heating block was made of graphite and had a Whatmann cartridge heater, regulated with a Pt-Rh cartridge heater. A temperature of 360 °C was required for the depositions. The AACVD rig was bound by a cylindrical quartz tube. A piezoelectric ultrasonic humidifier produced an aerosol which was transported to the rig by an N_2 carrier gas with a gas flow rate of 1 L min^{-1} for 40 min. After this time, more ethyl acetate (10 cm^3) was added to the precursor and deposited for 10 min. The total deposition length was 50 min. The rig was cooled in N_2 until it was <100 °C. The films deposited on the glass top plate (substrate) were translucent.

Deposition of TiO_2 Films on the Superhydrophobic Films Via AACVD: The superhydrophobic films underwent plasma surface treatment for 4 min with a gas flow of 2 sccm. Then, the superhydrophobic film was inserted into the same setup previously used. This time, the superhydrophobic film was placed on the carbon block. A glass top plate (substrate) was inserted into the rig to collect potential deposits. Titanium(IV) isopropoxide (varying volumes) was dissolved in anhydrous toluene (40 cm^3) and deposited onto the film when the preferred temperature of 350 °C was achieved. The deposition continued until the precursor in the humidifier stopped misting; at this point, the reactor was cooled in N_2 until it was <100 °C before the film deposited on the bottom plate was then handled in air. The films were denoted as: SH/TiO_2/x where "SH" refers to superhydrophobic and "x" was the volume of titanium(IV) isopropoxide used. Table 1 states the volumes of titanium(IV) isopropoxide used. The bottom plates varied from translucent (due to the superhydrophobic film underneath) to grey with rainbows stretching across parts of the film which became more prominent as the concentration of TTIP increased.

Instrumental Conditions: The same area was chosen for characterisation for each film which was closest to the inlet of the AACVD rig to ensure consistency. The sections of the film closest to the inlet had the thickest TiO_2 films.

A Thermo Scientific spectrometer with a mono-chromated Al-K alpha source (8.3381 Å) was used for X-ray photoelectron spectroscopy data, with peaks modeled on CasaXPS Version 2.3.25. Adventitious carbon (285.0 eV) was used as a charge reference. The JSM-7600F Scanning Electron Microscope (SEM) with an accelerating voltage of 5–20 keV was used to study the film's morphologies. All samples were vacuum-sputtered with carbon for 9 s prior to imaging to enhance the electrical conductivity of the films. The size of the particles in the SEM images was measured using ImageJ software Version 1.52s. Energy dispersive X-ray spectroscopy (EDS) was then carried out using an Oxford Instruments EDS system with scans varying in length from 10 min – 20 min. A Bruker alpha platinum instrument (wavenumber range: 400–4000 cm^{-1}) was used to carry out Attenuated Total Reflection Fourier-Transform Infrared Spectroscopy (FTIR-ATR). A Shimadzu UV-2700 spectrophotometer (wavelength range: 400 – 800 nm) was used to for collection of Ultraviolet spectroscopy (UV–vis) data. The films were exposed to a range of wavelengths (i.e., 400–800 nm, visible light), and percentage transmittance values were recorded. A mean of these percentage transmittance values across the wavelength range was taken and recorded for each film.

X-ray diffraction (XRD) was carried out using a Malvern PANalytical Empyrean Grazing Incidence-PXRD with parallel beam X-ray mirror for Cu radiation and a Xe point detector with a monochromated Cu Kα source operated at 40 kV with 40 mA emission current. The incident beam angle was set at 1°, and the 2θ range of 20°–65° was measured with a step size of 0.05° at 0.5 (s/step). A Raman spectrum was measured for each film using a Bruker Senterra II Raman Spectrometer with a wavelength of 532 nm and a power intensity of 25 mW.

The root-mean-square-height (Sq) of the films was measured with a Keyence VHX -S750E Optical Microscope, with x1500 magnification and Gaussian filter type but without an S-filter or L-filter. A Filmetrics F20 thin-film analyzer was used to determine the thickness of the TiO_2 films deposited on FTO float glass substrates.

The water contact angles (WCAs) were measured by dispensing 10 deionized (DI) water droplets of ≈5 µL and calculated using ADVANCE Version 1.14.3. This was carried out on a Kruss DSA 25E drop-shape analyzer with errors determined as one standard deviation. The contact angle hysteresis (CAH) was calculated using the sessile drop method; the advancing contact angle (ACA) was subtracted from the receding contact angle (RCA). The water contact angles of all the angles were measured using the Young–Laplace equation. The tilted drop method was used to measure the sliding angles (SAs). ≈15 µL water droplets were dropped onto the substrate after inclining the stage.

The photocatalytic activity of the films was measured by dipping them overnight in a solution of 0.05 M stearic acid (with chloroform as the solvent). The back of the films was cleaned with acetone and isopropanol before being exposed to UV light in a sealed box for up to 30 h, with FT-IR scans taken at regular intervals using a PerkinElmer Fourier transform Lambda RX I spectrometer over a wavelength range of 2700–3000 cm^{-1}. The corrected area in the range of 2800–3000 cm^{-1} was used, and converted into stearic acid coverage percentages and the errors were the initial standard deviations, propagated through the calculations.

Self-Cleaning Tests: Methylene blue dye was pipetted onto the materials, inclined at a 20° angle. Photographs of the films were captured to determine the water repellency of the films.

Durability—Ultraviolet Stability Test: Sections of the films were placed in a closed 365 nm Ultraviolet (UV) light box with an intensity of 260 mW cm^{-2} at room temperature for 15 days. Water contact angles were determined at regular intervals.

Durability—Heat Stability Test: Sections of the film were placed in a furnace at 300 °C for 5 h with water contact angles measured before and after heating.

Durability—Polarity Stability Test: Samples were submerged in solvents ethanol (polar) and toluene (apolar). Water contact angles were recorded at 1 h intervals for 5 h.

Durability—Tape Peel Test: Scotch Magic Tape was attached to and detached from the coatings 400 times, with water contact angles measured after every 5 cycles, then 10 cycles, and finally 25 cycles.

Durability—Pencil Hardness Test: The ASTM D3363 method was employed using the Elcometer 501 Pencil Hardness Tester (Elcometer Ltd, UK) to determine the films' maximum tolerable hardness. Pencils of increasing hardness (6H – 6B) were tested by pushing these across the film's surface at a 45° angle until a clean and well-defined line could be observed in the coating.

Supporting Information

Supporting Information is available from the Wiley Online Library or from the author.

Acknowledgements

J.J.K. is grateful to Dr. Jamie A. Gould for his help with the XRD characterization and analysis, the EPSRC (EP/N509577/1 and EP/T517793/1), and UCL Chemistry for its funding and support.

Conflict of Interest

The authors declare no conflict of interest.

Author Contributions

J.J.K. produced and characterized all films. J.J.K. wrote the manuscript with contributions from C.J.C. and C.S.B. The work was supervised by C.J.C. and C.S.B. All authors contributed to scientific discussions throughout the work.

© 2024 The Author(s). Advanced Materials Interfaces published by Wiley-VCH GmbH

21967350, 2024, 35, Downloaded from https://advanced.onlinelibrary.wiley.com/doi/10.1002/admi.202400519 by Test, Wiley Online Library on [23/07/2025]. See the Terms and Conditions (https://onlinelibrary.wiley.com/terms-and-conditions) on Wiley Online Library for rules of use; OA articles are governed by the applicable Creative Commons License

Data Availability Statement

The data that support the findings of this study are available from the corresponding author upon reasonable request.

Keywords

photocatalytic self-cleaning films, superhydrophobic, surface modification

Received: June 11, 2024
Revised: July 22, 2024
Published online: August 13, 2024

[1] J. Huo, C. I. De Leon Reyes, J. J. Kalmoni, S. Park, G. B. Hwang, S. Sathasivam, C. J. Carmalt, *ACS Appl. Nano Mater.* **2023**, *6*, 16383.
[2] Y. Wang, Z. Huang, R. S. Gurney, D. Liu, *Colloids Surfaces A.* **2019**, *561*, 101.
[3] W. Chen, W. Wang, D. X. Luong, J. T. Li, V. Granja, P. A. Advincula, C. Ge, Y. Chyan, K. Yang, W. A. Algozeeb, C. F. Higgs, J. M. Tour, *ACS Appl. Mater. Interfaces.* **2022**, *14*, 35053.
[4] Y. Cao, X. Liu, L. Zhang, Y. Wu, C. You, H. Li, H. Duan, J. Huang, P. Lv, *ACS Appl. Mater. Interfaces.* **2024**, *16*, 16973.
[5] W. Barthlott, C. Neinhuis, *Planta.* **1997**, *202*, 1.
[6] F. Xiao, S. Yuan, B. Liang, G. Li, S. O. Pehkonen, T. Zhang, *J. Mater. Chem. A.* **2015**, *3*, 4374.
[7] Y. Wang, X. Yao, S. Wu, Q. Li, J. Lv, J. Wang, L. Jiang, *Adv. Mater.* **2017**, *29*, 1.
[8] V. Jokinen, E. Kankuri, S. Hoshian, S. Franssila, R. H. A. Ras, *Adv. Mater.* **2018**, *30*, 1705104.
[9] K. Li, C. Wang, F. Gong, C. F. Cheung, Z. Chen, Z. Wang, *ACS Appl. Mater. Interfaces.* **2024**, *16*, 15548.
[10] F. Sotoudeh, S. M. Mousavi, N. Karimi, B. J. Lee, J. Abolfazli-Esfahani, M. K. D. Manshadi, *Alexandria Eng. J.* **2023**, *68*, 587.
[11] J. Jeevahan, M. Chandrasekaran, G. Britto Joseph, R. B. Durairaj, G. Mageshwaran, *J. Coatings Technol. Res.* **2018**, *15*, 231.
[12] J. J. Kalmoni, F. L. Heale, C. S. Blackman, I. P. Parkin, C. J. Carmalt, *Langmuir.* **2023**, *39*, 7731.
[13] X. Zhou, W. He, J. Ou, Y. Hu, F. Wang, X. Fang, W. Li, A. Amirfazli, *Colloids Surfaces A Physicochem. Eng. Asp.* **2024**, *689*, 133750.
[14] H. Yong, Z. Li, X. Huang, K. Wang, Y. N. Zhou, Q. Li, J. Shi, M. Liu, D. Zhou, *Adv. Mater. Interfaces.* **2022**, *9*, 1.
[15] W. H. Huang, C. S. Lin, *Appl. Surf. Sci.* **2014**, *305*, 702.
[16] Z. Geng, J. He, L. Yao, *RSC Adv.* **2015**, *5*, 89262.
[17] N. Bai, Q. Li, H. Dong, C. Tan, P. Cai, L. Xu, *Chem. Eng. J.* **2016**, *293*, 75.
[18] P. N. Wani, S. K. Kale, S. S. Dahiwale, U. T. Nakate, S. U. Ekar, Y. T. Nakate, P. S. More, M. T. Sarode, Y. B. Khollam, *Mater. Sci. Eng. B.* **2023**, *288*, 116212.
[19] K. Wang, S. Yu, W. Li, Y. Song, P. Gong, M. Zhang, H. Li, D. Sun, X. Yang, X. Wang, *Appl. Surf. Sci.* **2022**, *595*, 153565.
[20] G. Shukla, C. Kumar, S. Angappane, *Phys. Status Solidi Basic Res.* **2019**, *256*, 1.
[21] Y. Cao, A. Salvini, M. Camaiti, *Constr. Build. Mater.* **2023**, *404*, 133139.
[22] Y. Nosaka, A. Y. Nosaka, *J. Phys. Chem. Lett.* **2016**, *7*, 431.
[23] R. Guo, Y. Bao, X. Zheng, J. Chen, H. Yang, W. Zhang, C. Liu, J. Xu, *ACS Appl. Mater. Interfaces.* **2023**, *15*, 47447.
[24] J. H. Lee, E. J. Park, D. H. Kim, M. Jeong, Y. D. Kim, *Catal. Today.* **2016**, *260*, 32.
[25] A. Ansari, N. M. Nouri, *Ceram. Int.* **2023**, *49*, 57.
[26] C. E. Knapp, C. J. Carmalt, *Chem. Soc. Rev.* **2016**, *45*, 1036.
[27] A. Tombesi, S. Li, S. Sathasivam, K. Page, F. L. Heale, C. Pettinari, C. J. Carmalt, I. P. Parkin, *Sci. Rep.* **2019**, *9*, 1.
[28] K. J. Heo, J. H. Yoo, J. Shin, W. Huang, M. K. Tiwari, J. H. Jung, I. P. Parkin, C. J. Carmalt, G. B. Hwang, *J. Mater. Chem. A.* **2024**, *12*, 3886.
[29] V. Diesen, M. Jonsson, I. P. Parkin, *Chem. Vap. Depos.* **2013**, *19*, 355.
[30] J. Liu, L. Ye, S. Wooh, M. Kappl, W. Steffen, H. J. Butt, *ACS Appl. Mater. Interfaces.* **2019**, *11*, 27422.
[31] S. Wahyuningsih, R. E. Cahyono, F. N. Aini, A. H. Ramelan, *Bull. Chem. React. Eng. Catal.* **2020**, *15*, 874.
[32] X. J. Guo, C. H. Xue, S. Sathasivam, K. Page, G. He, J. Guo, P. Promdet, F. L. Heale, C. J. Carmalt, I. P. Parkin, *J. Mater. Chem. A.* **2019**, *7*, 17604.
[33] S. Ashraf, C. S. Blackman, G. Hyett, I. P. Parkin, *J. Mater. Chem.* **2006**, *16*, 3575.
[34] W. E. Slink, P. B. DeGroot, *J. Catal.* **1981**, *68*, 423.
[35] L. L. Larina, O. Omelianovych, V. D. Dao, K. Pyo, D. Lee, H. S. Choi, *Nanoscale.* **2021**, *13*, 175.
[36] P. Vitanov, P. Stefanov, A. Harizanova, T. Ivanova, *J. Phys. Conf. Ser.* **2008**, *113*, 2.
[37] S. Praserthdam, M. Rittiruam, K. Maungthong, T. Saelee, S. Somdee, P. Praserthdam, *Sci. Rep.* **2020**, *10*, 1.
[38] P. Praveen, G. Viruthagiri, S. Mugundan, N. Shanmugam, *Spectrochim. Acta - Part A Mol. Biomol. Spectrosc.* **2014**, *117*, 622.
[39] A. Chae, S. Doo, D. Kim, T. Y. Ko, T. Oh, S. J. Kim, D. Y. Koh, C. M. Koo, *Langmuir.* **2022**, *38*, 12657.
[40] S. Vudayagiri, M. D. Junker, A. L. Skov, *Polym. J.* **2013**, *45*, 871.
[41] O. V. Almjasheva, *Nanosyst. Physics, Chem. Math.* **2016**, *7*, 1031.
[42] Q. Liu, J. Yu, H. Wang, *Int. J. Heat Mass Transf.* **2020**, *148*, 118985.
[43] R. Quesada-Cabrera, A. Mills, C. O'Rourke, *Appl. Catal. B Environ.* **2014**, *150*, 338.
[44] I. Dundar, A. Mere, V. Mikli, M. Krunks, I. O. Acik, *Catalysts.* **2020**, *10*, 1.
[45] A. Vahl, S. Veziroglu, B. Henkel, T. Strunskus, O. Polonskyi, O. C. Aktas, F. Faupel, *Materials (Basel).* **2019**, *12*, 2840.
[46] H. Nadeem, A. M. Waterhouse, G. I. N. Idriss, *Catal. Today.* **2012**, *182*, 16.
[47] R. Gorthy, A. Wasa, J. G. Land, Z. Yang, J. A. Heinemann, C. M. Bishop, S. P. Krumdieck, *Surf. Coatings Technol.* **2021**, *409*, 126857.
[48] S. A. Campbell, R. C. Smith, *High-K Gate Dielectr.* **2003**, *1*, 65.
[49] P. Fu, J. Ou, Y. He, Y. Hu, F. Wang, X. Fang, W. Li, A. Amirfazli, *Surfaces and Interfaces.* **2024**, *45*, 103890.

© 2024 The Author(s). Advanced Materials Interfaces published by Wiley-VCH GmbH

21967350, 2024, 35, Downloaded from https://advanced.onlinelibrary.wiley.com/doi/10.1002/admi.202400519 by Test, Wiley Online Library on [23/07/2025]. See the Terms and Conditions (https://onlinelibrary.wiley.com/terms-and-conditions) on Wiley Online Library for rules of use; OA articles are governed by the applicable Creative Commons License